Research in Astronomy and Astrophysics, 23:085016 (9pp), 2023 August https://doi.org/10.1088/1674-4527/acd995

Detection of the Milky Way Reflex Motion Caused by the Magellanic Clouds in Different Observation Accuracy

Ya-Nan Cao[1,2,3], Hao Tian[4,5*], Shi Shao[4], Xiang-Xiang Xue[2,5], Yi-Zhou Liu[3], Zhou Fan[2,3], and Jing Li[1*]

[1] School of Physics and Astronomy, China West Normal University, Nanchong 637009, China; lijing@bao.ac.cn
[2] CAS Key Laboratory of Optical Astronomy, National Astronomical Observatories, Chinese Academy of Sciences, Beijing 100101, China
[3] School of Astronomy and Space Science, University of Chinese Academy of Sciences, Beijing 100049, China
[4] Key Laboratory of Space Astronomy and Technology, National Astronomical Observatories, Chinese Academy of Sciences, Beijing 100101, China
[5] Institute for Frontiers in Astronomy and Astrophysics, Beijing Normal University, Beijing, 102206, China; tianhao@nao.cas.cn
Received 2023 March 20; revised 2023 May 19; accepted 2023 May 23; published 2023 July 5

Abstract

Motivated by recent studies of the perturbation of the Magellanic Clouds (MCs) on the Milky Way (MW) and the planned multi-band wide-field deep survey named Chinese Space Station Telescope (CSST), we explore the detection limit of the MW reflex motion due to the MCs infall in different observation precision using an MW-MCs-mass galaxy from MAGPIE simulation to provide a reference for the CSST survey. By involving different errors of distance, proper motion, and radial velocity, we investigate the reflex motion characterized by the velocity shift in each velocity component. We find the strongest shifts in the tangential velocities, which align with the motion direction of the MCs. In the ideal case that distance errors dominate, we find a relative distance error of 10% can allow the reliable detection of velocity shifts in tangential velocities within 100 kpc, and a relative distance error of 30% is the minimum requirement to detect the reliable tangential velocity shifts of about 40 km s^{-1} within 50 kpc. Different errors of proper motions in combination with a relative distance error of 10% or 20% show an error of 0.1 mas yr^{-1} in proper motions can guarantee the reliable detection of velocity shifts in V_l and V_b up to 80–100 kpc and an error of 0.15 mas yr^{-1} is the minimum requirement. In the other ideal case that radial velocity errors dominate, we find a radial velocity error of 20 km s^{-1} can present reliable reflex motion in line-of-sight velocity up to 70 kpc, while the detection volume will be reduced to 50 kpc as the radial velocity error increases to 40 km s^{-1}. When the radial velocity error is larger than 60 km s^{-1}, the velocity shifts cannot be detected anymore. In addition, we find that reliable detection of reflex motion requires at least 20% of the whole sample.

Key words: Galaxy: kinematics and dynamics – (galaxies:) Magellanic Clouds – Galaxy: halo

1. Introduction

Magellanic Clouds (MCs), composed of the Large Magellanic Cloud (LMC) at a distance of ∼50 kpc and the Small Magellanic Cloud (SMC) at ∼61 kpc, are the closest pair of dwarf galaxies to our Milky Way (MW). In recent years, a myriad of evidence shows that the mass of LMC is about $\sim10^{11}M_\odot$, which is more massive than it was believed to be (van der Marel et al. 2009; Kallivayalil et al. 2013; van der Marel & Kallivayalil 2014; Peñarrubia et al. 2016; Shao et al. 2018). About 1/10 of the MW mass cannot be neglected, so the gravitational forces exerted by the MCs are ubiquitously felt by the MW.

The infall of such a massive LMC can have a significant impact on the MW. Many new phenomena have been proposed, including the reflex motion of the MW in response to the LMC (Gómez et al. 2015; Erkal et al. 2019, 2020; Petersen & Peñarrubia 2020, 2021), the deflections of Galactic streams due to the gravitational tug from the LMC (Erkal et al. 2018, 2019), and the LMC wake in the MW halo (Gómez et al. 2016; Garavito-Camargo et al. 2019; Conroy et al. 2021).

LMC challenges the equilibrium of the Milky Way, which prompts the study of *N*-body MW simulations including LMC. Gómez et al. (2015) pointed out that the MW center-of-mass can be dislodged significantly as a response to the LMC infall. The resulting reflex motion of the Milky Way is an all-sky effect. The fits to the Orphan stream reveal this could be ∼50 km s^{-1} (Erkal et al. 2019). The first observational evidence of reflex motion was reported by Petersen & Peñarrubia (2021). They found that the MW center-of-mass is moving at ∼32 km s^{-1} detected in the velocities of outer halo stars and MW satellite galaxies. The reflex motion is also reflected directly in the velocity shifts of Galactic tracers beyond 30 kpc (Erkal et al. 2020, 2021).

Therefore, obtaining the kinematics of stars beyond 50 kpc is of particular importance. The Chinese Space Station Telescope (CSST) is a planned large space astronomy telescope built by China Manned Space. The CSST is a 2 m space telescope with a large field of view of 1.1 deg^2 and a shared orbit with the

* Corresponding authors.

Chinese Space Station, covering a large sky area of 17,500 $\deg^2$ with a high spatial resolution of $\sim 0\farcs15$ (Sun et al. 2021). The CSST covers the near-UV-visible-near-infrared band and has a limit of 26 mag for multi-band imaging survey and 23 mag for the slitless spectroscopic survey (resolution $R > 200$). It is designed to survey 40% of the sky in 10 yr, resolving individual stars in the galaxies within several Mpc. Precise stellar parameters from the slitless spectra from CSST will provide invaluable distances (and proper motions) of stars from 50 to 100 kpc range.

In this work, we investigate the reliable detection of the velocity shifts given different precision of *observables*, and the dependence on the sample size, based on an MW-MCs simulation. In Section 2, we describe the MW-MCs simulation, the selection of the "MW-halo" sample, and the addition of observation errors. Then we show the velocity shifts detected in different observation errors, directions and sample sizes to conclude the detection limits in Section 3. Finally, we summarize our results in Section 4.

2. Data

To test the detection of reflex motion of the MW-mass galaxy due to its MCs-mass satellite galaxies under different observation accuracy, we select an MW-mass simulated galaxy from the zoom-in hydrodynamical MAGPIE simulations (S. Shao et al. 2023, in preparation), which is accompanied by a pair of satellite galaxies with LMC and SMC masses (hereafter MW-MCs simulation). The detailed selection criteria of the MW-MCs simulation are described in Section 2.1. Then we project the simulation box x, y, z, v_x, v_y, v_z to the observation space to involve in the observation errors. Specifically, by assuming the Sun's position and motion in the simulation, we first project the simulation onto the observation space relative to the Sun using position and velocity parameters, including distance modulus (DM), galactic longitude (l), galactic latitude (b), radial velocity (RV), and proper motions (μ_l, μ_b). We then add different observation errors to produce the *"observables."* Finally we calculate the velocities and positions of the stars using those *"observables."*

2.1. MW-MCs Simulation

The MW-MCs simulation is a simulated galaxy system that is most like our MW and MCs, selected from the MAGPIE simulations. The MAGPIE project consists of five halos which are selected from a cosmological simulation, Ref-L0100N1504, from the Eagle Project (Schaye et al. 2015) that has a periodic box of a side length of 100 Mpc and contains roughly a thousand MW-mass halos. The halos in the MAGPIE simulations have an averaged total mass of $\sim 10^{12}\,M_\odot$ which is consistent with the inferred mass of our MW halo (e.g., Wang et al. 2020). Particularly, the MW-MCs simulation is also required to have a pair of satellite galaxies in the virial radius of the host galaxy, which is similar to the observed features of our MW-MCs system (S. Shao et al. 2023, in preparation). The simulations presented were performed with the code developed for the EAGLE project. The galaxy formation models of the simulations include radiative cooling, star formation, stellar evolution and stellar mass-loss, and thermal feedback that captures the collective effects of stellar winds, radiation pressure, and supernova explosions. The simulation assumes a Planck cosmology (Planck Collaboration et al. 2014) with cosmological parameters: $\Omega_\mathrm{m} = 0.307$ (total matter density), $\Omega_\mathrm{b} = 0.04825$ (baryon density), $\Omega_\Lambda = 0.693$ (dark energy density), $h = 0.6777$ (the Hubble constant at present in units of $100\,\mathrm{km\,s^{-1}\,Mpc^{-1}}$), $\sigma_8 = 0.8288$ (the rms amplitude of linear mass fluctuations in spheres of $8\,h^{-1}$ Mpc comoving radius at redshift $z = 0$) and $n_\mathrm{s} = 0.9611$ (the spectral index of the primordial power spectrum). Each halo in MAGPIE simulations was run at multiple resolution levels. The typical dark matter particle and gas cell mass resolutions for MAGPIE simulations are $1.2 \times 10^5\,M_\odot$ and $6.6 \times 10^6\,M_\odot$, respectively. We make use of the first MAGPIE halo in which the host galaxy is accompanied by a pair of satellite galaxies with stellar masses of $4.4 \times 10^9\,M_\odot$ and $1.1 \times 10^9\,M_\odot$ and infall total masses of 1.0×10^{11} and 6.0×10^{10}, which are most similar to the masses of LMC and SMC. LMC-mass satellite has an infall lookback time of $t_\mathrm{infall} = 2.7$ Gyr and has passed its first pericenter 1.8 Gyr ago ($r_\mathrm{peri} \sim 50$ kpc). The spatial distribution of the star particles of the MW-MCs simulation is shown in Figure 1. The relative positions of the three simulated galaxies are also similar to our MW-MCs system. The reflex motion characterized by $\langle V\rangle(r)$ of the host galaxy of the MW-MCs simulation is different from that simulated by Erkal et al. (2020) since they used an idealized simulation without having a cosmological context such as galaxy mergers, but the order of magnitude of the velocity shifts are similar to their results (about tens of kilometers per second in velocity shift).

In the MW-MCs simulation, we select the members of the satellites using an earlier snapshot when they were still bound to the satellite. Figure 1 shows the spatial distribution of all-star particles in the MW-MCs simulation. The MCs-mass galaxy are represented by the red and blue dots in the top panels. In the bottom panels, the star particles tagged as MW-mass galaxy are shown.

2.2. Projection to the Observation Space

Broadly speaking, the observables of a star are the sky positions, multi-band apparent magnitudes, parallax, proper motions, radial velocity, stellar atmospheric parameters, and chemical abundances etc. Different surveys provide different observables. Taking CSST for example, the main survey project of CSST includes two parts, the multi-band imaging survey and the slitless spectroscopic survey, which can provide the sky positions, multi-band magnitudes, radial velocities and stellar atmospheric parameters.

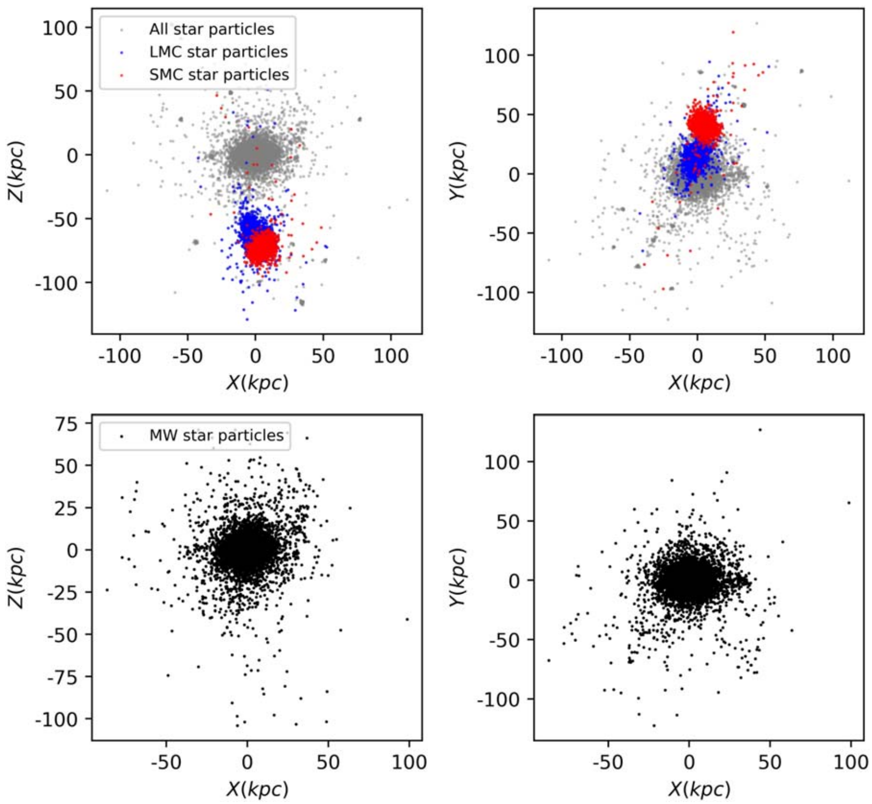

Figure 1. The spatial distribution of all star particles and MW star particles. The top row illustrates all of the simulated star particles, represented by gray dots. The blue and red dots denote particles belonging to the LMC-mass and SMC-mass simulated galaxies, respectively. The bottom row displays star particles of MW-mass simulated galaxy.

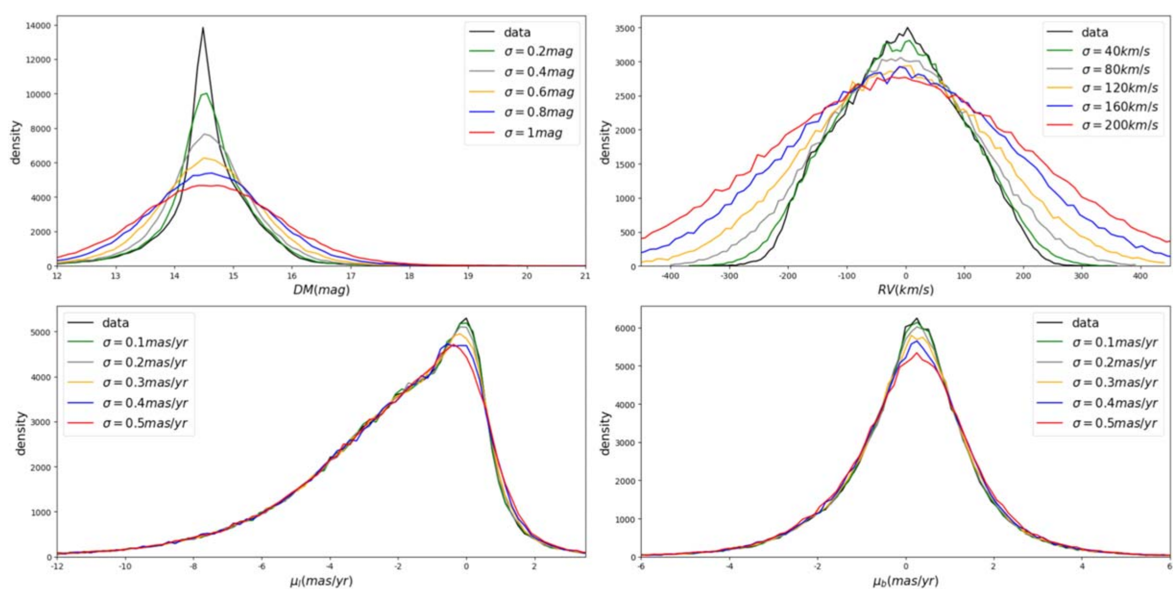

Figure 2. The distribution of the distance modulus DM, heliocentric radial velocity (RV), and proper motions (μ_l, μ_b) before and after adding errors. The black lines represent the data before the error was added.

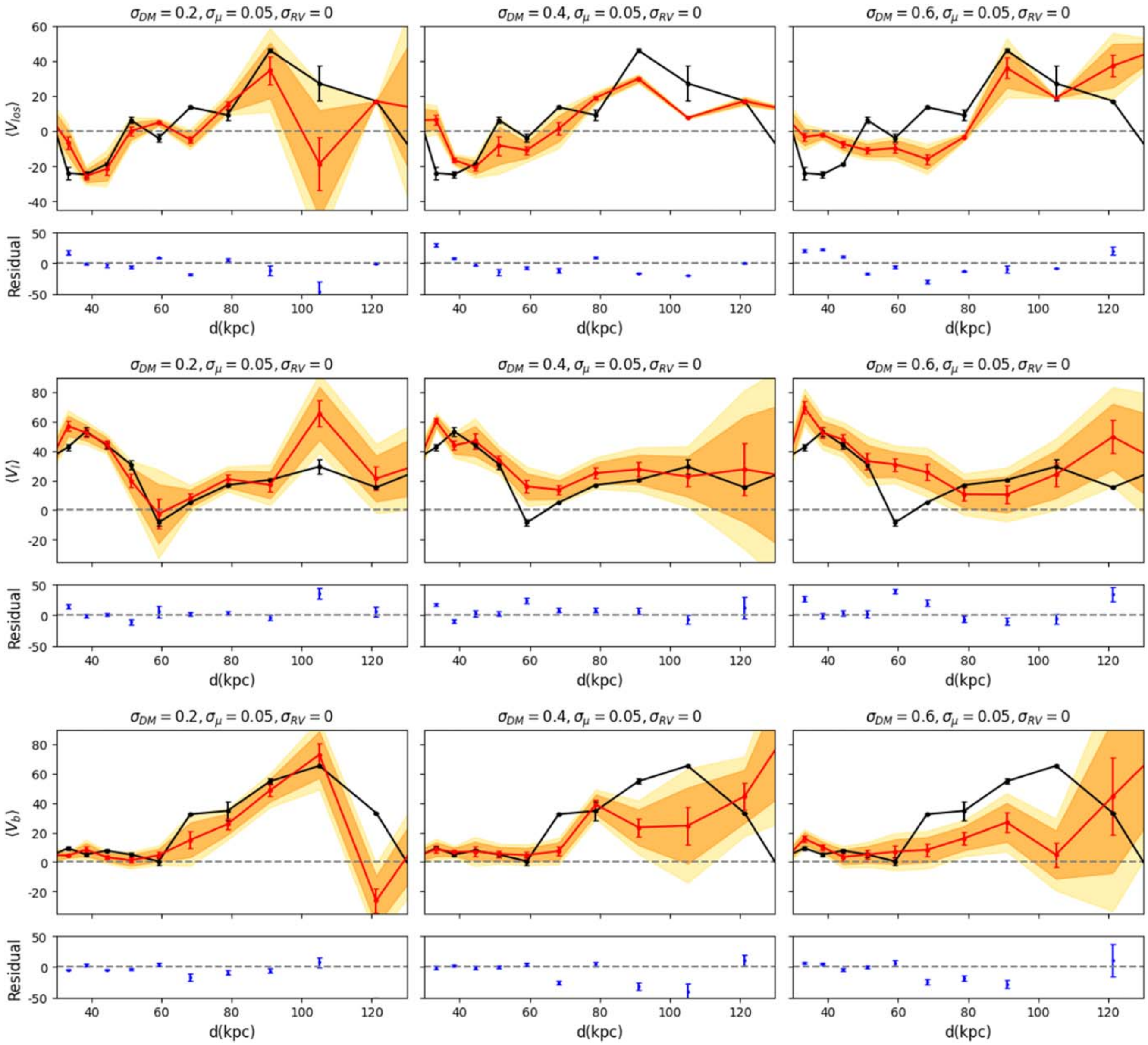

Figure 3. The effects of distance errors on the mean velocities of $V_{\rm los}$, V_l, and V_b. Three vertical panels show the velocity shifts with different errors of DM, while three horizontal panels show velocity shifts of different velocity components. The black line is the mean velocity without adding error, and the red lines show the mean velocity after involving errors of DM. The color bands show 2σ and 3σ regions.

The distances of some stars can be determined based on multi-band magnitudes and stellar atmospheric parameters. The proper motions are possible to obtain through the synergy with other surveys. Therefore, the kinematics related observables provided by CSST are DM, l, b, RV, μ_l, and μ_b.

To investigate the detection of the reflex motion under different observation accuracy and provide reference for CSST, the simulation box x, y, z, v_x, v_y, v_z should be projected to DM, l, b, RV, μ_l, μ_b. By locating the "Sun" in the simulation with position $(X_\odot, Y_\odot, Z_\odot) = (8, 0, 0)$ kpc, we find the velocity of the "Sun" is $(V_{x,\odot}, V_{y,\odot}, V_{z,\odot}) = (-11.1, 109.5, -4.7)\ {\rm km\ s^{-1}}$. We can then use the following procedure to project the MW-MCs simulations into the observation space

$$\begin{cases} d = \sqrt{(X - X_\odot)^2 + Y^2 + Z^2} \\ l = \tan^{-1}\dfrac{Y}{X - X_\odot} \\ b = \sin^{-1}\dfrac{Z}{d} \end{cases} \tag{1}$$

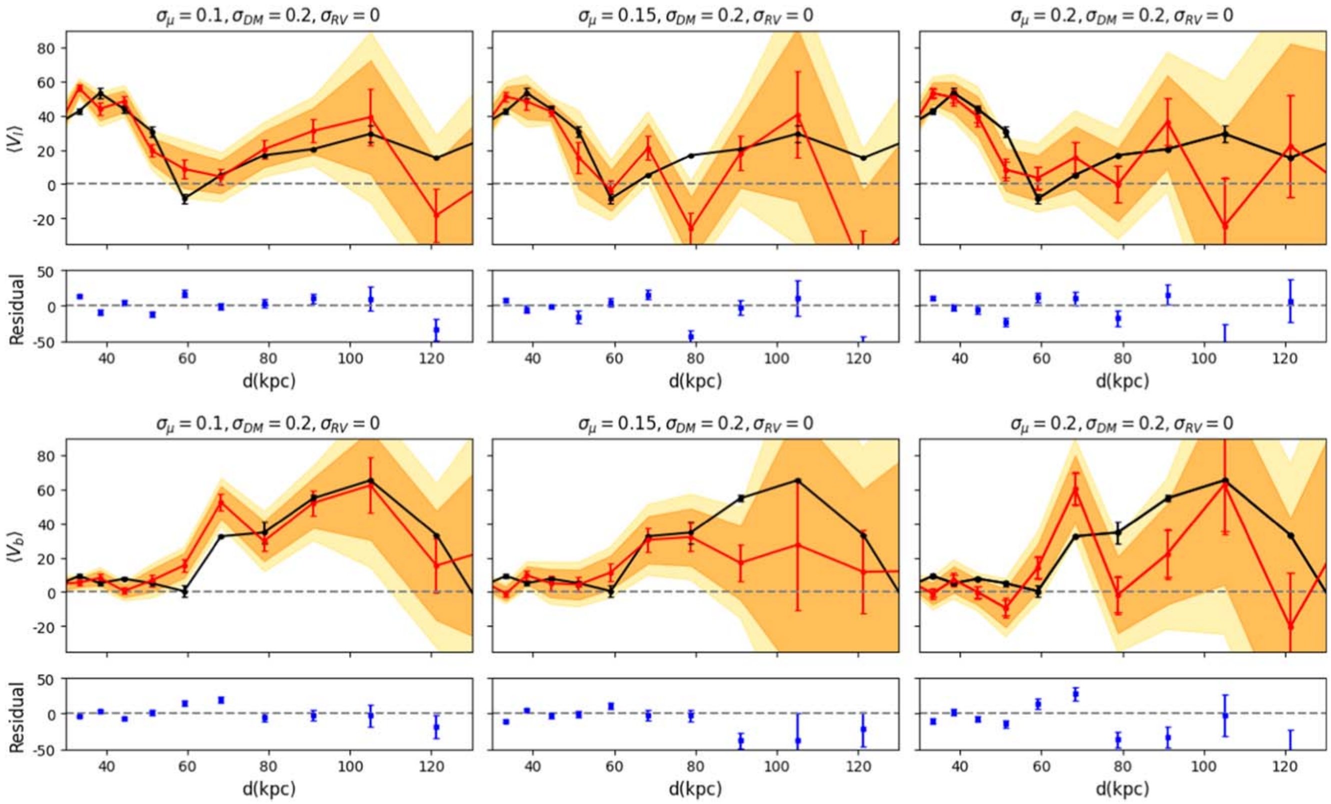

Figure 4. Effects of proper motion errors on the mean velocities in V_l and V_b. The DM error is 0.2 mag and RV error is 0. The black line shows the result without adding error, while the red line represents the result after adding errors. The color bands show 2σ and 3σ regions of the red lines.

where d is the distance to the Sun in kpc, l and b are the Galactic longitude and latitude in degree, respectively. Here we use distance modulus $\mathrm{DM} = 5(\log_{10} d - 2)$ instead of the distance because the errors of the apparent magnitudes and absolute magnitudes can be propagated to DM easily.

The proper motions and radial velocity can be calculated by

$$\begin{bmatrix} RV \\ 4.74 \cdot d \cdot \mu_l \\ 4.74 \cdot d \cdot \mu_b \end{bmatrix} = \boldsymbol{A} \cdot \begin{bmatrix} V_x \\ V_y \\ V_z \end{bmatrix} - \boldsymbol{A} \cdot \begin{bmatrix} V_{x,\odot} \\ V_{y,\odot} \\ V_{z,\odot} \end{bmatrix} \tag{2}$$

where

$$\boldsymbol{A} = \begin{bmatrix} \cos l \cos b & -\sin l & -\cos l \sin b \\ \sin l \cos b & \cos l & -\sin l \sin b \\ \sin b & 0 & \cos b \end{bmatrix}. \tag{3}$$

2.3. Errors of the Observables

To evaluate the detection of the reflex motion, different errors of distances, radial velocities, and proper motions are added to the simulation. The choices of the error range for different observables are based on literature and the properties of CSST.

The ideal stellar tracers to map the MW halo should be bright enough to be observed in the distant halo, so the K giants, blue-horizontal-branch stars and RR Lyrae stars have long been used to study our MW halo. K giants are the most prominent stars in the halo with a typical distance error of $\sim$20% (Xue et al. 2014), equivalent to a distance modulus error of $\sim$0.4 mag ($\delta_d/d = 0.46 \times \delta_{\mathrm{DM}}$) derived from the low-resolution spectroscopic surveys such as SDSS and LAMOST. As standard candles, blue horizontal branch stars (BHBs) and RR Lyrae stars (RRLs) have better distances, with a typical distance error of <10% for BHBs (Xue et al. 2008) and 3% $\sim$ 5% for RRLs (Bhardwaj 2020). The equivalent distance modulus errors are $\sim$0.2 mag and $\sim$0.1 mag for BHBs and RRLs respectively. Considering deep surveys such as CSST may have larger errors on the distance estimations, we choose the DM errors ranging from 0.1 to 1.0 mag (equivalent distance errors ranging from 5% to 50%) to evaluate the detection of the reflex motion.

Radial velocity is obtained from the spectrum, and its accuracy is proportional to the resolution and signal-to-noise ratio (S/N) of the spectrum. A typical radial velocity error is about $10\ \mathrm{km\ s^{-1}}$ for low resolution ($R \sim 2000$) spectroscopic survey, such as LAMOST and SDSS. CSST is planned to take

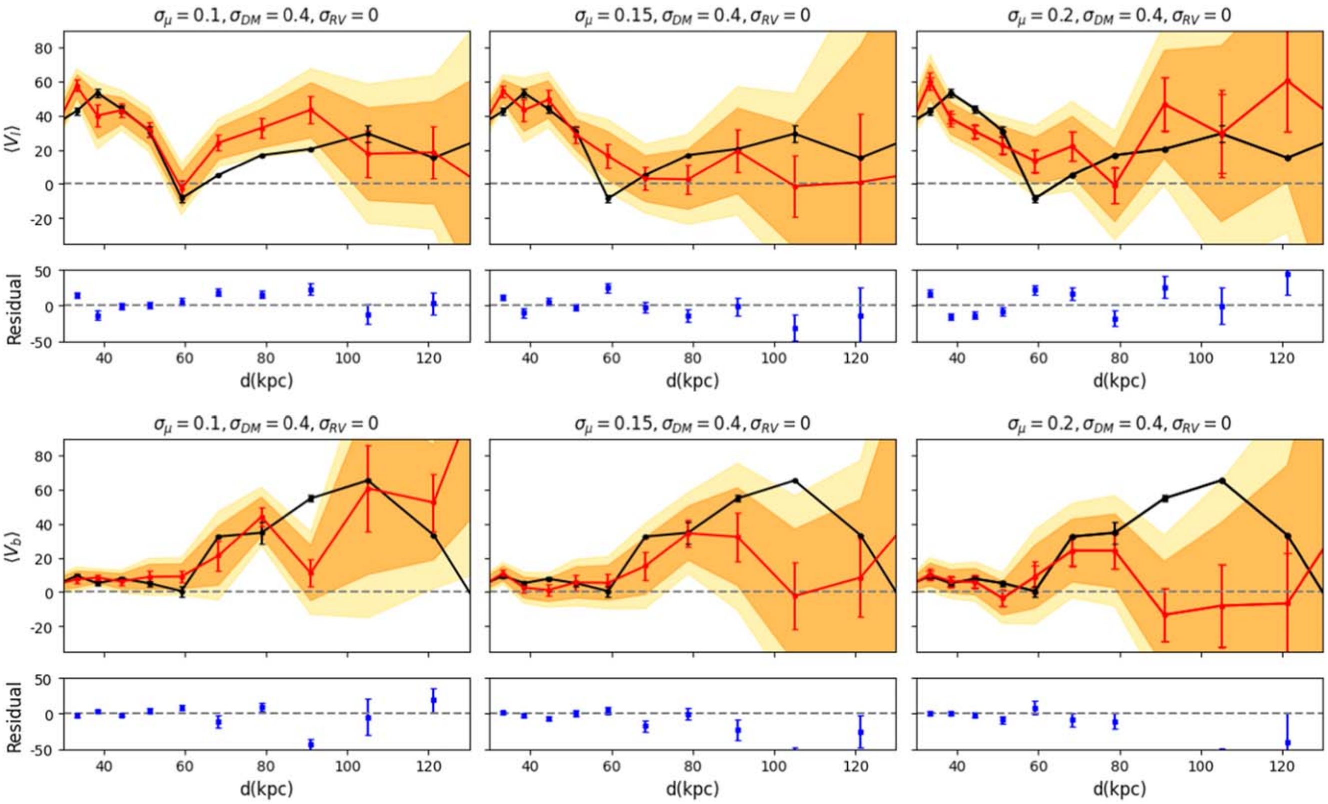

Figure 5. Same as Figure 4, but the DM error is 0.4 mag.

slitless spectra for stars brighter than $g = 23$ mag with resolution $R > 200$. Sun et al. (2021) predicted that the well-calibrated slitless spectra with an S/N of 100 enable a typical radial velocity error of about 3 km s^{-1} for AFGKM stars and about 10 km s^{-1} for OB stars. However, the ideal cases are always a minority. Due to the very low resolution of the slitless spectra, it is possible to give larger errors of radial velocities for most stars. Therefore, we choose the errors of radial velocities ranging from 20 to 200 km s^{-1}.

Proper motions can only be obtained from multi-epoch observation with a long enough time baseline. Gaia can provide the best proper motions of stars for now with an error <0.5 mas yr^{-1} for stars brighter than 20 mag. Though CSST is not designed to do the astrometry survey to provide the proper motions, a combination with previous surveys enables measurements of the proper motions at higher accuracy than Gaia with a longer time baseline, especially for the faint stars. Taking care of the worst case, we adopt the errors of the proper motions ranging from 0.05 to 0.5 mas yr^{-1}. Please note that we have incorporated the same error value for μ_l and μ_b.

We use 10 equally spaced errors within each error range. The errors are randomly produced from a Gaussian distribution with a center of 0 and a sigma of the given error. Then we add the errors to the simulation to construct 10 samples with errors from small to large. Please note that we assume the quality of the data is related to each observable to avoid making grid in error space. The distributions of the DM, RV, μ_l and μ_b with different errors are shown in Figure 2.

3. Results

The reflex motion induced by the MCs' infall can be explored by the mean velocity in radial shells. If there are no MCs, the MW stellar halo is in equilibrium, so the mean velocity is close to zero. But MCs' infall breaks the equilibrium and leads to the shifts of the mean velocities $\langle V_x \rangle$, $\langle V_y \rangle$, $\langle V_z \rangle$ from zero beyond 30 kpc, especially in the z direction (Erkal et al. 2020). Here we adopt a set of spherical coordinate (d, l, b). Most of the time, we cannot have all three velocity components. The coordinate of (d, l, b) is centered at the Sun, where the observables can be separated completely to investigate the effect from individual observables. Based on the 10 samples with different errors constructed in Section 2, we transfer DM, l, b, RV, μ_l, μ_b to $V_{\rm los}$, V_l, V_b, d and then computing the mean velocities in different distance bins to construct "observed" velocity shifts. Here all velocities are in Galactic standard of rest. The influence of the observables' errors on the detection of reflex motion is investigated by comparing the "observed" velocity shifts with the "real"

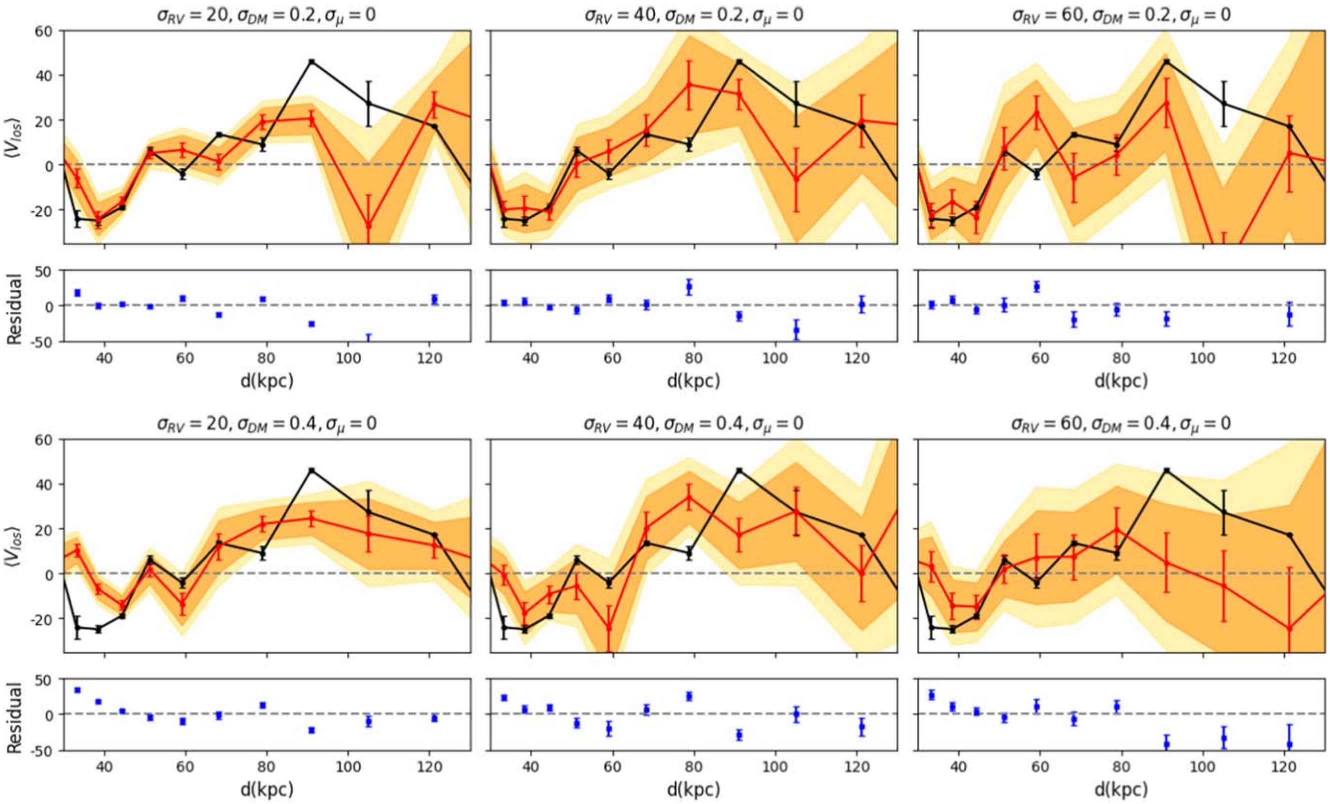

Figure 6. The effect of RV errors on the mean velocity in $V_{\rm los}$. The DM error is either 0.2 mag or 0.4 mag, and there is no error in the proper motions. The black line is the velocity shifts without adding error, and the red line is the velocity shifts with errors. The color bands are 2σ and 3σ errors.

velocity shifts that do not involve any errors. In order to quantitatively describe how similar the "observed" velocity shifts are to the "real" velocity shifts, we define "reliable detection" as the case that the "real" velocity shifts lie within 2σ errors of the "observed" velocity shifts. The observed errors of the mean velocities are propagated from the errors of observables by Monte Carlo sampling. The statistical errors of the mean velocities are derived from bootstrap resampling. We add the observed errors in quadrature to the statistical errors to get 1σ errors of the mean velocities. In this section, we will describe the detection of the reflex motion in different observation accuracy in detail.

3.1. The Effect from DM Errors

The distance is essential to convert proper motions to tangential velocities. Furthermore, the reflex motion investigated here is characterized by the mean velocity shifts varying with distances. Therefore, when we explore the influence of the distances' errors, a current typical error of proper motion needs to be considered. Gaia DR3 has provided proper motions better than $0.04\,{\rm mas\,yr^{-1}}$ for stars brighter than $G = 15$ mag and $0.1\,{\rm mas\,yr^{-1}}$ for stars brighter than $G = 17$ mag. In future, the precision of proper motion will be improved as the increase of the observation baseline. As a result, we take an ideal precision of proper motion as $0.05\,{\rm mas\,yr^{-1}}$.

Assuming no error in RV, an error of $0.05\,{\rm mas\,yr^{-1}}$ in proper motion, and an arithmetic sequence of 10 DM errors ranging from 0.1 to 1.0 mag, we then calculate the mean velocities ($V_{\rm los}$, V_l, V_b) of the star particles located at various d, ranging from 30 to 130 kpc.

Figure 3 shows the mean velocity shifts in each velocity component for three representative cases of DM errors. We find stronger velocity shifts in V_l, and V_b than that in $V_{\rm los}$, which is consistent with the moving direction of LMC-mass galaxy. An oscillation in velocity shifts is found in $V_{\rm los}$ and V_l, which could be due to the fact that LMC-mass galaxy has passed its first pericenter in simulation, while in reality, LMC has been approaching its first pericenter. When DM errors are 0.2 mag, the "observed" velocity shifts of $\langle V_l \rangle$ and $\langle V_b \rangle$ show very good consistent with "real" velocity shifts to about 100 kpc, while reliable detection of the $\langle V_{\rm los} \rangle$ shifts only can be traced to 50 kpc. With the increase of DM errors to 0.6 mag, it is impossible to detect any reliable velocity shifts in $\langle V_{\rm los} \rangle$, but the reliable detection of shifts in $\langle V_l \rangle$ and $\langle V_b \rangle$ still can be traced to about 50 kpc. The stronger the velocity shifts, the greater the admissible margin of error in observations.

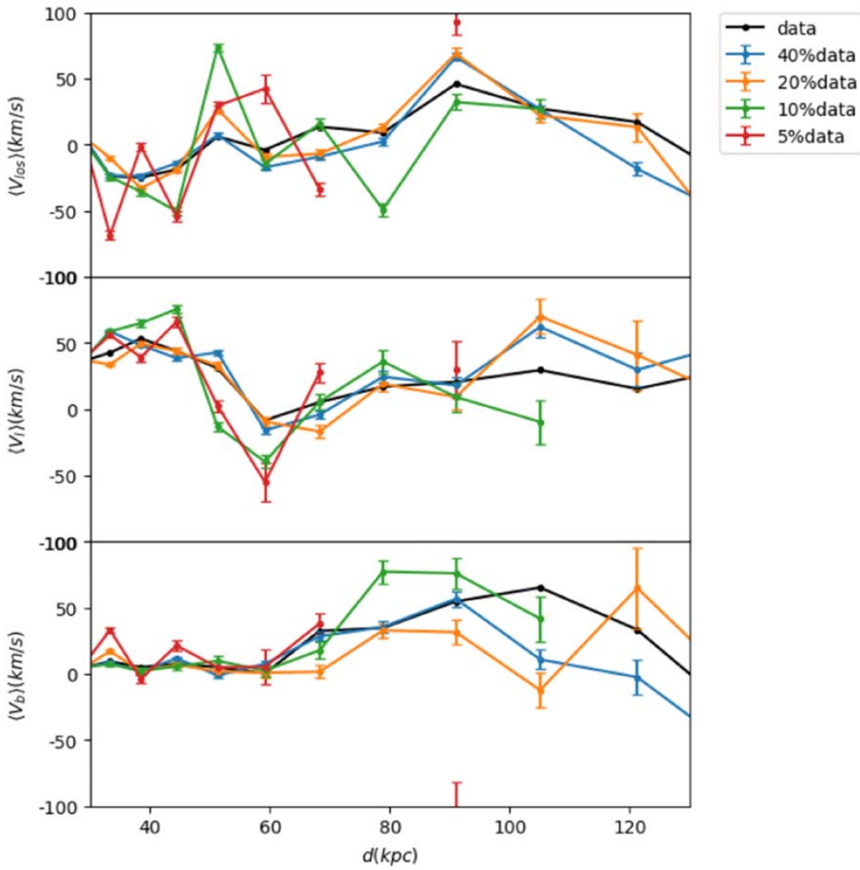

Figure 7. The mean velocity distribution along the distance for different sample sizes. The solid black line represents the mean velocity of the simulated data without errors. We show the four data sets as color lines (blue: 40% of the sample size; orange: 20% of the sample size; green: 10% of the sample size; red: 5% of the sample size). All subsamples are added ideal errors.

Moreover, the larger the observation error, the closer the distance from which reliable velocity shifts can be detected. From the above tests, we find that a DM error of 0.6 mag is a minimum requirement to detect reliable tangential velocity shifts of about 40 km s^{-1} within 50 kpc.

3.2. The Effect from Proper Motion Errors

In Section 3.1 we have found that the errors of DM should not be worse than 0.6 mag, so we test the effect of proper motion errors by adopting two typical DM errors of 0.2 and 0.4 mag (corresponding to a relative distance error of ∼10% for BHB stars and ∼20% for RGB stars). We adopt 10 errors of the proper motions from 0.05 to 0.5 mas yr^{-1}, and show 3 representative cases in Figures 4 and 5. When DM errors are 0.2 mag, a proper motion error of 0.15 mas yr^{-1} allows reliable detection on velocity shifts in both $\langle V_l\rangle$ and $\langle V_b\rangle$ up to 60 kpc, and a proper motion error of 0.1 mas yr^{-1} extends the reliable detection distance region up to about 100 kpc (shown as Figure 4). When the distance errors are getting large to 20%, a proper motion error of 0.1 mas yr^{-1} can guarantee the reliable detection of velocity shifts in $\langle V_b\rangle$ to 80 kpc and in $\langle V_l\rangle$ to 60 kpc, while a proper motion error of 0.15 mas yr^{-1} allows reliable detection of shifts in $\langle V_l\rangle$ to about 50 kpc. Therefore, when the stellar distances are accurate to 10% ∼ 20%, a proper motion of 0.15 mas yr^{-1} is the minimum requirement to trace reliable tangential velocity shifts.

3.3. The Effect from RV Errors

We investigate the impact of RV errors on the detection of velocity shifts by setting the DM errors to 0.2 and 0.4 mag, the proper motion errors to 0, and the RV error to 0–200 km s^{-1}. Figure 6 shows that an RV error of 20 km s^{-1} can trace reliable velocity shifts to about 70 kpc for both cases of DM errors. When DM error is 0.2 mag, the RV error of 40 km s^{-1} still can show reliable detection to 50 kpc. When the error of RV increases to 60 km s^{-1}, velocity shifts cannot be detected.

3.4. The Effect from the Sample Size

Limited by the observational depth of all surveys, it is impossible to obtain all the stars in the Galactic halo. Therefore, we perform the results of experiments with randomly selected subsamples of 40%, 20%, 10%, and 5% from the full simulated sample to investigate the effect of sample size on the detection of reflex motion. For the subsamples, we involve a DM error of 0.1 mag, a proper motion error of 0.05 mas yr^{-1}, an RV error of 10 km s^{-1}. As shown in Figure 7, the black line indicates the mean velocity distribution traced with all the samples without errors. While the results with different fractions of the whole sample are represented by different color lines. The subsample containing 40% of the whole sample shows the velocity profiles are able to be traced well to 90 kpc. If there is only 20% of the whole sample, the reliable detection of velocity shifts can be traced to 60 kpc. With lower fractions, the samples are unable to trace the outer volumes because of the low number of samples with larger distances. On the other hand, even in the inner volume with lower fractions, the profile becomes more fluctuated because of the stronger Poisson noise. As a result, 20% of the sample size is the minimum requirement on the detection of reflex motion.

4. Summary

The Milky Way and the LMC are in disequilibrium and, in particular, the LMC pushes the outer parts of our galaxy out of equilibrium (Erkal et al. 2019). In this study, we demonstrate that the LMC should be perturbative to our MW halo, showing signs of global motion for areas beyond 30 kpc. We propose the minimum requirements for the errors of observables to be able to detect reliable reflex motions, which could be a reference for surveys to evaluate the potential to study the reflex motion.

(i) The minimum requirement on DM error is 0.6 mag. For DM errors below 0.6 mag (30% in distance error), the reliable detection of shifts in tangential velocities can be traced to 50 kpc, while nearly no reliable velocity shifts in $V_{\rm los}$ can be detected. When the distances are good to 10% (0.2 mag in DM error), we can detect reliable reflex motion in tangential velocities up to 100 kpc and in line-of-sight velocity up to 50 kpc.

(ii) The minimum requirement on proper motion error is 0.15 mas yr^{-1}. The mean tangential velocities $\langle V_l \rangle$ and $\langle V_b \rangle$ can reflect the real velocity shift up to about 100 kpc if the relative error of distance is $\sim$10% and the error of proper motion is less than 0.1 mas yr^{-1}. When the errors of proper motions increase to 0.15 mas yr^{-1}, the reliable reflex motion can be detected to about 50–60 kpc for stars with distances accurate to 10% $\sim$ 20%.

(iii) The minimum requirement on RV error is 40 km s^{-1}. An RV error of 20 km s^{-1} allows us to detect reliable reflex motion to 70 kpc when the distances are better than 20%. When the DM error is 0.2 mag, the RV error of 40 km s^{-1} still can show reliable detection to 50 kpc. When the error of RV increases to 60 km s^{-1}, velocity shifts cannot be detected anymore.

(iv) A sample size of 20% or more is required to reflect the true velocity shift.

Acknowledgments

This work is supported by the National Key Research and Development Program of China No. 2019YFA0405504, the science research grants from the China Manned Space Project with NO. CMS-CSST-2021-B03, the National Natural Science Foundation of China (NSFC) grant Nos. 11988101, 11890694, 12103062, 12273027, 12273053 and 12173046, and CAS Project for Young Scientists in Basic Research grant No. YSBR-062. S.S. acknowledges support from the K. C. Wong Foundation. J.L. would like to acknowledge the Sichuan Youth Science and Technology Innovation Research Team (grant No. 21CXTD0038), and the Innovation Team Funds of China West Normal University (grant No. KCXTD2022-6).

ORCID iDs

Hao Tian https://orcid.org/0000-0003-3347-7596
Shi Shao https://orcid.org/0000-0001-8382-6323
Xiang-Xiang Xue https://orcid.org/0000-0002-0642-5689
Yi-Zhou Liu https://orcid.org/0009-0005-8855-0748
Jing Li https://orcid.org/0000-0002-4953-1545

References

Bhardwaj, A. 2020, JApA, 41, 23
Conroy, C., Naidu, R. P., Garavito-Camargo, N., et al. 2021, Natur, 592, 534
Erkal, D., Belokurov, V., Laporte, C. F. P., et al. 2019, MNRAS, 487, 2685
Erkal, D., Belokurov, V. A., & Parkin, D. L. 2020, MNRAS, 498, 5574
Erkal, D., Deason, A. J., Belokurov, V., et al. 2021, MNRAS, 506, 2677
Erkal, D., Li, T. S., Koposov, S. E., et al. 2018, MNRAS, 481, 3148
Garavito-Camargo, N., Besla, G., Laporte, C. F. P., et al. 2019, ApJ, 884, 51
Gómez, F. A., Besla, G., Carpintero, D. D., et al. 2015, ApJ, 802, 128
Gómez, F. A., White, S. D. M., Marinacci, F., et al. 2016, MNRAS, 456, 2779
Kallivayalil, N., van der Marel, R. P., Besla, G., Anderson, J., & Alcock, C. 2013, ApJ, 764, 161
Peñarrubia, J., Gómez, F. A., Besla, G., Erkal, D., & Ma, Y.-Z. 2016, MNRAS, 456, L54
Petersen, M. S., & Peñarrubia, J. 2020, MNRAS, 494, L11
Petersen, M. S., & Peñarrubia, J. 2021, NatAs, 5, 251
Planck Collaboration, Ade, P. A. R., Aghanim, N., et al. 2014, A&A, 571, A16
Schaye, J., Crain, R. A., Bower, R. G., et al. 2015, MNRAS, 446, 521
Shao, S., Cautun, M., Deason, A. J., Frenk, C. S., & Theuns, T. 2018, MNRAS, 479, 284
Sun, Y., Deng, D.-S., & Yuan, H.-B. 2021, RAA, 21, 092
van der Marel, R. P., & Kallivayalil, N. 2014, ApJ, 781, 121
van der Marel, R. P., Kallivayalil, N., & Besla, G. 2009, in IAU Symp., 256, The Magellanic System: Stars, Gas, and Galaxies, ed. J. T. Van Loon & J. M. Oliveira (Cambridge: Cambridge Univ. Press), 81
Wang, W., Han, J., Cautun, M., Li, Z., & Ishigaki, M. N. 2020, SCPMA, 63, 109801
Xue, X.-X., Ma, Z., Rix, H.-W., et al. 2014, ApJ, 784, 170
Xue, X. X., Rix, H. W., Zhao, G., et al. 2008, ApJ, 684, 1143